A numerical approach based on variational methods to an elastodynamic contact problem

Sci. Rep. Kanazawa Univ.
Vol. 63, pp. 29–44, 2019

ARTICLES

A numerical approach based on variational methods to an elastodynamic contact problem

Yoshiho AKAGAWA,[1]* Shuichi MORIKAWA,[2] Seiro OMATA[1]

[1]Graduate School of Natural Science and Technology, Kanazawa University,
Kakuma, Kanazawa 920-1192, Japan
[2] PFU Limited, Unoke, Kahoku 929-1192, Japan

(Received December 25, 2018 and accepted in revised form February 12, 2019)

Abstract We investigate a rolling contact problem in elastodynamics. Contact problems in elasticity appear in various fields such as manufacturing and earthquake engineering. In particular, we have in mind the application to printers, where paper sheets are driven through the printer by rollers. A typical problem for such printers is that the roller may produce a squeaking sound. As a step towards preventing such a sound, we study a simplified model in which the roller is modeled as an elastic body driven by a rotation. The paper sheet is modeled as a rigid obstacle. For simplicity, we assume no frictional forces between the roller and the obstacle. The resulting equations of motion are of hyperbolic type with a free boundary. The aim of the paper is to develop a numerical scheme to solve these equations of motion. The scheme is based on a variational method called the discrete Morse flow. The novelty is that this scheme has not been applied to a hyperbolic system with a free boundary where the unknown function is vector-valued.

Keywords. dynamical rolling contact problem, hyperbolic free boundary problem, discrete Morse flow

1 Introduction

Rolling contact problems appear throughout manufacturing wherever gears and tires are involved. We focus on the application to printers, where the rolling contact occurs at the place (sheet feeder) where the paper sheets are taken inside the printer. The sheet feeder consists of rubber rollers which move the paper sheets through the printer. The problem with such sheet feeders is that they may produce a squeaking sound. This sound is caused by the contact of the rubber rollers with the paper sheets. In this paper, we work towards solving the problem of this squeaking sound by modeling the dynamics of the rubber rollers by elastodynamics.

Several earlier attempts have been made to model the dynamics of rollers. The first simplified model is introduced by Signorini [1], who models the rollers as static, linear elastic bodies subjected to a frictionless rigid obstacle. The Signorini problem was formulated and analyzed mathematically by [2] as a variational problem. To allow for large deformations, this model was

*Corresponding author Email: yoshiho.akagawa@gmail.com

extended to nonlinear elasticity and analyzed numerically by [4, 5]. There, the authors studied the equations for the steady state of a rolling hyperelastic material in contact with an obstacle by Coulomb friction, and implemented a numerical scheme for it. However, the steady-state solutions cannot explain the squeaking sound. It remains difficult to solve the rolling contact problem by using the equation of elastodynamics, because the related set of equations contain a free boundary, are of hyperbolic nature, and are nonlinear due to the use of hyperelasticity to allow for large deformations.

Therefore, our aim is to extend the numerical scheme for the stationary setting in [4, 5] to a dynamical scheme. Since it is difficult to treat at once the free boundary, hyperbolic dynamics and the nonlinearities that come with hyperelasticity, we will use instead the equations of linear elasticity in the coordinate frame which rotates along with the roller. The resulting equations are of hyperbolic type with a free boundary.

Our numerical scheme is based on the discrete Morse flow (DMF), which was introduced in [8]. The DMF is a variational method based on a minimizing movement scheme which was intended for parabolic type problems. The application of DMF is extended in [9] to problems of hyperbolic type. It is further extended in [10] so that hyperbolic problems with free boundaries can be treated. The key idea is to put the obstacle constraint as a restriction on the admissible set over which the energy functional related to the DMF is minimized.

However, the case of scalar-valued functions is treated in [10], while the application of the DMF to our setting requires the extension to vector-valued functions. The aim of this paper is therefore to extend the DMF to vector-valued functions. We demonstrate the use of this extension by applying it to a rolling contact problem.

The paper is organised as follows. In Section 2 we derive the set of equations (P) for the rolling contact problem. In Section 3 we apply the discrete Morse flow to develop a numerical scheme (P_k) for (P). In Section 4 we solve (P_k) numerically and discuss the application to the rolling contact problem.

2 Governing equations

In this section, we introduce our notation and the set of governing equations (P).

2.1 Geometry

Let $\Omega \subset \mathbb{R}^2$ be a bounded domain representing the area occupied by an elastic body. The closure $\overline{\Omega}$ of the set Ω is called the reference configuration. We denote by $\boldsymbol{\varphi} : \overline{\Omega} \to \mathbb{R}^2$ the deformation of the reference configuration $\overline{\Omega}$, and refer to $\boldsymbol{\varphi}(\overline{\Omega})$ as the deformed configuration. We call the components of $\boldsymbol{x}$ Lagrangian coordinates, and the components of $\boldsymbol{X} = \boldsymbol{\varphi}(\boldsymbol{x})$ Eulerian coordinates (see Figure 1) in the deformed configuration.

At each point $\boldsymbol{x} \in \Omega$, the deformation gradient is given by

$$\boldsymbol{F}(\boldsymbol{x}) := \nabla \boldsymbol{\varphi}(\boldsymbol{x}) = \begin{pmatrix} \dfrac{\partial \varphi_1}{\partial x_1}(\boldsymbol{x}) & \dfrac{\partial \varphi_1}{\partial x_2}(\boldsymbol{x}) \\ \dfrac{\partial \varphi_2}{\partial x_1}(\boldsymbol{x}) & \dfrac{\partial \varphi_2}{\partial x_2}(\boldsymbol{x}) \end{pmatrix}.$$

We require that the determinant of the deformation gradient is positive at all points of the reference configuration, that is

$$J(\boldsymbol{x}) := \det \boldsymbol{F}(\boldsymbol{x}) > 0$$

for all $\boldsymbol{x} \in \Omega$. As a consequence, the matrix $\boldsymbol{F}(\boldsymbol{x})$ is invertible.

Before linearizing, we describe the equations for mechanical equilibrium in terms of nonlinear elasticity. The Cauchy stress tensor $\boldsymbol{T} = (T_{ij})$ is defined in the deformed configuration by

$$\boldsymbol{T}(\boldsymbol{X}) := \frac{1}{J(\boldsymbol{x})} \left\{ \mu \left(\boldsymbol{F}(\boldsymbol{x}) \boldsymbol{F}^T(\boldsymbol{x}) - \boldsymbol{I} \right) + \frac{\lambda}{2} \left(J(\boldsymbol{x})^2 - 1 \right) \boldsymbol{I} \right\} \tag{2.1}$$

for all $\boldsymbol{x} \in \Omega$, where $\boldsymbol{X} = \boldsymbol{\varphi}(\boldsymbol{x})$, μ and λ are the Lamé constants ($\lambda + \mu \geq 0$, $\mu > 0$), the matrix $\boldsymbol{F}^T(\boldsymbol{x})$ is the transpose of $\boldsymbol{F}(\boldsymbol{x})$, and $\boldsymbol{I}$ is the identity matrix.

In our model for the roller, the deformation naturally decomposes as

$$\boldsymbol{\varphi} = \boldsymbol{R}(\mathbf{id} + \boldsymbol{\xi}) \quad \text{in } \Omega, \tag{2.2}$$

where the matrix $\boldsymbol{R} = (R_{ij})$ describes the counter-clockwise rotation by angle θ (see Figure 1), $\mathbf{id} : \mathbb{R}^2 \to \mathbb{R}^2$ denotes the identity map, and $\boldsymbol{\xi} : \Omega \to \mathbb{R}^2$ is assumed to have small derivatives. More precisely, we assume that

$$\left| \frac{\partial \xi_i}{\partial x_j}(\boldsymbol{x}) \right| < \varepsilon, \qquad \left| \frac{\partial^2 \xi_i}{\partial x_j \partial \xi_k}(\boldsymbol{x}) \right| < \varepsilon \tag{2.3}$$

for some $\varepsilon > 0$ small enough, uniformly with respect to $\boldsymbol{x} \in \Omega$ and $1 \leq i, j, k \leq 2$.

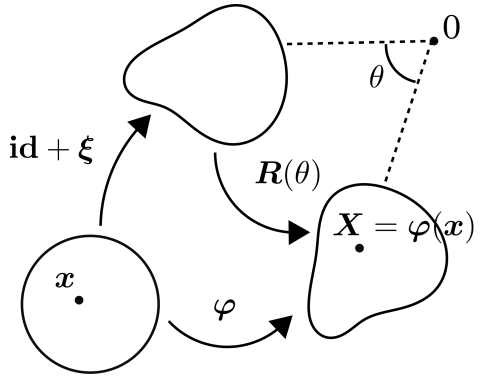

Figure 1: Sketch of the decomposition of the deformation $\boldsymbol{\varphi}$.

2.2 Equations of motion

To derive the equations of motion, we change variables in (2.1) by writing it in terms of $\boldsymbol{\xi}$ on Ω, and expand it in terms of ε by relying on (2.3). Since $\nabla \boldsymbol{\xi}$ plays the role of the deformation in linearized elasticity, we introduce the strain tensor

$$\boldsymbol{\varepsilon}[\boldsymbol{\xi}] := \frac{1}{2} \left(\nabla \boldsymbol{\xi} + \nabla \boldsymbol{\xi}^T \right)$$

and the stress tensor

$$\boldsymbol{\sigma}[\boldsymbol{\xi}] := 2\mu \boldsymbol{\varepsilon}[\boldsymbol{\xi}] + \lambda (\operatorname{div} \boldsymbol{\xi}) \boldsymbol{I}$$

in the reference configuration. The Cauchy stress tensor $\boldsymbol{T}(\boldsymbol{X})$ in Lagrangian coordinates is given by

$$\begin{aligned}
T_{ij} &= \frac{1}{J}\left\{\mu\left[R_{ik}\left(\delta_{k\ell}+\frac{\partial\xi_k}{\partial x_\ell}\right)\left(\delta_{m\ell}+\frac{\partial\xi_m}{\partial x_\ell}\right)R_{jm}-\delta_{ij}\right]+\frac{\lambda}{2}\left[\Big(1+\operatorname{div}\boldsymbol{\xi}+\det(\nabla\boldsymbol{\xi})\Big)^2-1\right]\delta_{ij}\right\}\\
&= \frac{1}{J}\left\{\mu R_{ik}\left(\frac{\partial\xi_k}{\partial x_m}+\frac{\partial\xi_m}{\partial x_k}+\frac{\partial\xi_k}{\partial x_\ell}\frac{\partial\xi_m}{\partial x_\ell}\right)R_{jm}\right.\\
&\quad\left.+\frac{\lambda}{2}\left[2\Big(\operatorname{div}\boldsymbol{\xi}+\det(\nabla\boldsymbol{\xi})\Big)+\Big(\operatorname{div}\boldsymbol{\xi}+\det(\nabla\boldsymbol{\xi})\Big)^2\right]R_{ik}\delta_{km}R_{jm}\right\}\\
&= \frac{1}{J}R_{ik}\sigma_{km}[\boldsymbol{\xi}]R_{jm}+\frac{1}{J}R_{ik}\left\{\mu\frac{\partial\xi_k}{\partial x_\ell}\frac{\partial\xi_m}{\partial x_\ell}+\frac{\lambda}{2}\left[2\det(\nabla\boldsymbol{\xi})+\Big(\operatorname{div}\boldsymbol{\xi}+\det(\nabla\boldsymbol{\xi})\Big)^2\right]\delta_{km}\right\}R_{jm}.
\end{aligned}$$

Here and henceforth we use the convention to sum over repeated indices. Then, the divergence of the tensor $\boldsymbol{T}$ reads as

$$\begin{aligned}
(\mathbf{div}_{\boldsymbol{X}}\boldsymbol{T})_i := \frac{\partial T_{ij}}{\partial X_j} &= R_{ik}\left(\frac{1}{J}\frac{\partial}{\partial x_m}\sigma_{k\ell}[\boldsymbol{\xi}]-\frac{1}{J^2}\sigma_{k\ell}[\boldsymbol{\xi}]\frac{\partial J}{\partial x_m}\right)\frac{\partial(\boldsymbol{\varphi}^{-1})_m}{\partial x_j}R_{j\ell}+O(\varepsilon^2)\\
&= R_{ik}\left(1-\Big(\operatorname{div}\boldsymbol{\xi}+\det(\nabla\boldsymbol{\xi})\Big)+O(\varepsilon^2)\right)\frac{\partial}{\partial x_m}\sigma_{k\ell}[\boldsymbol{\xi}]R_{jm}R_{j\ell}+O(\varepsilon^2) \qquad (2.4)\\
&= R_{ik}\frac{\partial}{\partial x_\ell}\sigma_{k\ell}[\boldsymbol{\xi}]+O(\varepsilon^2),
\end{aligned}$$

where $\boldsymbol{\varphi}^{-1}$ is the inverse function of $\boldsymbol{\varphi}$.

Next we derive the equations of motion. We encode the forced rotation of the elastic body by a given smooth function $\theta:[0,T)\to\mathbb{R}$ that corresponds to the rotation angle of $\boldsymbol{R}$. Then, by (2.2), the now time-dependent fields $\boldsymbol{\varphi}:\overline{\Omega}\times[0,T)\to\mathbb{R}^2$ and $\boldsymbol{\xi}:\overline{\Omega}\times[0,T)\to\mathbb{R}^2$ satisfy

$$\boldsymbol{\varphi}(\boldsymbol{x},t)=\boldsymbol{R}(\theta(t))(\boldsymbol{x}+\boldsymbol{\xi}(\boldsymbol{x},t)) \qquad (2.5)$$

for all $\boldsymbol{x}\in\overline{\Omega}$ and all $t\geq 0$. After neglecting higher order terms of ε in (2.4), the conservation of linear momentum yields the equation of elastodynamics,

$$\rho\ddot{\boldsymbol{\varphi}}=\mathbf{div}_{\boldsymbol{X}}\boldsymbol{T}\approx\boldsymbol{R}(\theta)\,\mathbf{div}\,\boldsymbol{\sigma}[\boldsymbol{\xi}]\quad\text{in }\Omega\times(0,T),$$

where $\rho>0$ is the density, superposed dots denote partial differentiation with respect to time (i.e., $\ddot{\boldsymbol{\varphi}}:=\partial^2\boldsymbol{\varphi}/\partial t^2$), and

$$\mathbf{div}\,\boldsymbol{\sigma}:=\begin{pmatrix}\dfrac{\partial\sigma_{11}}{\partial x_1}+\dfrac{\partial\sigma_{12}}{\partial x_2}\\[2ex]\dfrac{\partial\sigma_{21}}{\partial x_1}+\dfrac{\partial\sigma_{22}}{\partial x_2}\end{pmatrix}. \qquad (2.6)$$

To write the left-hand side of (2.2) in terms of $\boldsymbol{\xi}$, we use (2.5) to compute

$$\begin{aligned}
\ddot{\boldsymbol{\varphi}} &= \ddot{\theta}\frac{d}{d\theta}\boldsymbol{R}(\theta)(\mathbf{id}+\boldsymbol{\xi})+\dot{\theta}^2\frac{d^2}{d\theta^2}\boldsymbol{R}(\theta)(\mathbf{id}+\boldsymbol{\xi})+2\dot{\theta}\frac{d}{d\theta}\boldsymbol{R}(\theta)\dot{\boldsymbol{\xi}}+\boldsymbol{R}(\theta)\ddot{\boldsymbol{\xi}}\\
&= \boldsymbol{R}(\theta)\left\{\ddot{\theta}\boldsymbol{R}(\pi/2)(\mathbf{id}+\boldsymbol{\xi})+\dot{\theta}^2\boldsymbol{R}(\pi)(\mathbf{id}+\boldsymbol{\xi})+2\dot{\theta}\boldsymbol{R}(\pi/2)\dot{\boldsymbol{\xi}}+\ddot{\boldsymbol{\xi}}\right\}\\
&= \boldsymbol{R}(\theta)\left\{-\ddot{\theta}\boldsymbol{R}(-\pi/2)(\mathbf{id}+\boldsymbol{\xi})-\dot{\theta}^2(\mathbf{id}+\boldsymbol{\xi})-2\dot{\theta}\boldsymbol{R}(-\pi/2)\dot{\boldsymbol{\xi}}+\ddot{\boldsymbol{\xi}}\right\}.
\end{aligned}$$

In the above calculation, we have used that $\frac{d}{d\theta}\boldsymbol{R}(\theta)=\boldsymbol{R}(\theta)\boldsymbol{R}(\pi/2)$. Inserting this result in (2.2), we obtain

$$\rho\ddot{\boldsymbol{\xi}}=\mathbf{div}\,\boldsymbol{\sigma}[\boldsymbol{\xi}]+\rho\left(\ddot{\theta}\boldsymbol{R}(-\pi/2)(\mathbf{id}+\boldsymbol{\xi})+\dot{\theta}^2(\mathbf{id}+\boldsymbol{\xi})+2\dot{\theta}\boldsymbol{R}(-\pi/2)\dot{\boldsymbol{\xi}}\right)\quad\text{in }\Omega\times(0,T). \qquad (2.7)$$

We note that if θ is linear in time, then, within the parentheses in the right-hand side, the first term vanishes, the second term is the centrifugal force, and the last term is the Coriolis force. To abbreviate the term in parentheses, we define the function $\boldsymbol{f}$ by

$$\boldsymbol{f}(t,\boldsymbol{x},\boldsymbol{\xi},\dot{\boldsymbol{\xi}}) := \ddot{\theta}(t)\boldsymbol{R}(-\pi/2)(\boldsymbol{x}+\boldsymbol{\xi}) + \dot{\theta}(t)^2(\boldsymbol{x}+\boldsymbol{\xi}) + 2\dot{\theta}(t)\boldsymbol{R}(-\pi/2)\dot{\boldsymbol{\xi}}. \tag{2.8}$$

We remark that the time dependence of the rotation angle is not covered by the setting in [3, 4].

2.3 Boundary conditions

We divide the boundary $\partial\Omega$ into Γ_D and Γ_C (see Figure 2), where

$$\Gamma_D \cup \Gamma_C = \partial\Omega, \quad \Gamma_D \cap \Gamma_C = \emptyset, \quad \Gamma_D \neq \emptyset.$$

On the boundary Γ_D we model the forced rotation of Ω by imposing the Dirichlet boundary condition

$$\boldsymbol{\varphi}(\boldsymbol{x}) = \boldsymbol{R}\boldsymbol{x} \quad \text{for } \boldsymbol{x} \in \Gamma_D,$$

which is equivalent to

$$\boldsymbol{\xi} = \boldsymbol{0} \quad \text{on } \Gamma_D.$$

We describe the height of the obstacle by a smooth function $g : [0,T) \to \mathbb{R}$. The condition that the deformed configuration remains above the obstacle is given by

$$\varphi_2(\boldsymbol{x}) = (\boldsymbol{x}+\boldsymbol{\xi}(\boldsymbol{x})) \cdot \left(\boldsymbol{R}^T\boldsymbol{e}_2\right) \geq g \quad \text{for all } \boldsymbol{x} \in \Gamma_C,$$

where $\boldsymbol{e}_i \in \mathbb{R}^2$ are the unit vectors of the canonical basis in the Lagrangian frame. We call

$$\{\boldsymbol{\varphi}(\boldsymbol{x}) ; \boldsymbol{x} \in \Gamma_C,\ \varphi_2(\boldsymbol{x}) = g\}$$

the contact zone, and note that it is an unknown subset of Γ_C.

Using the contact zone, we describe the boundary conditions on Γ_C. Outside of the contact zone, we impose homogeneous Neumann boundary conditions (i.e., zero traction). At the contact zone, we impose zero traction in tangential direction (i.e., no friction force between the elastic body and the obstacle), and require the normal force of the obstacle on the elastic body to be non-negative. This leads to the following boundary conditions on Γ_C:

$$\left\{ \begin{array}{r} (\mathbf{id}+\boldsymbol{\xi}) \cdot \left(\boldsymbol{R}^T\boldsymbol{e}_2\right) \geq g \\ (\boldsymbol{\sigma}[\boldsymbol{\xi}]\boldsymbol{n}) \cdot \left(\boldsymbol{R}^T\boldsymbol{e}_1\right) = 0 \\ (\boldsymbol{\sigma}[\boldsymbol{\xi}]\boldsymbol{n}) \cdot \left(\boldsymbol{R}^T\boldsymbol{e}_2\right) \geq 0 \\ \left((\mathbf{id}+\boldsymbol{\xi}) \cdot \left(\boldsymbol{R}^T\boldsymbol{e}_2\right) - g\right)(\boldsymbol{\sigma}[\boldsymbol{\xi}]\boldsymbol{n}) \cdot \left(\boldsymbol{R}^T\boldsymbol{e}_2\right) = 0 \end{array} \right\} \quad \text{on } \Gamma_C,$$

where $\boldsymbol{n}$ is the unit outward normal vector to Γ_C.

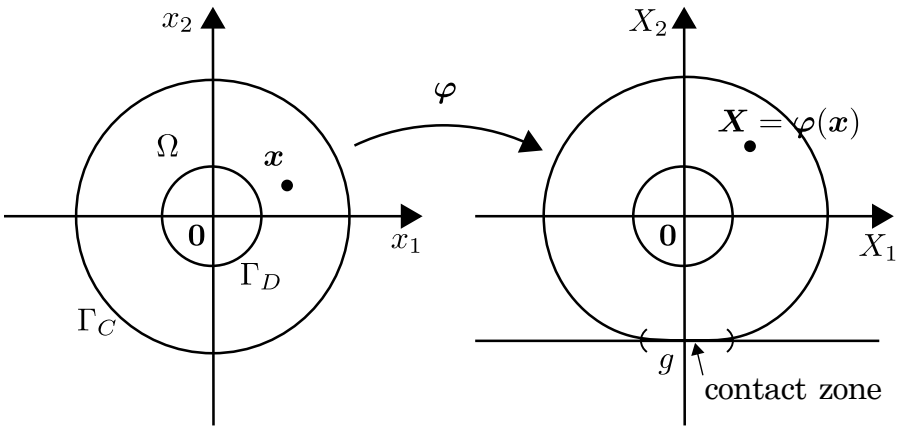

Figure 2: Sketch of the boundary components Γ_D, Γ_C and the contact zone.

2.4 Full model

Summarizing the equations above, and adding initial conditions, we obtain the complete system given by

$$
(\mathrm{P})\quad \begin{cases}
\rho\ddot{\boldsymbol{\xi}} - \mathbf{div}\,\boldsymbol{\sigma}[\boldsymbol{\xi}] = \rho \boldsymbol{f}(\cdot,\cdot,\boldsymbol{\xi},\dot{\boldsymbol{\xi}}) & \text{in} \quad \Omega\times(0,T),\\
\boldsymbol{\xi} = \mathbf{0} & \text{on} \quad \Gamma_D\times[0,T),\\
(\mathbf{id}+\boldsymbol{\xi})\cdot\big(\boldsymbol{R}^T(\theta)\boldsymbol{e}_2\big) \geq g & \text{on} \quad \Gamma_C\times[0,T),\\
(\boldsymbol{\sigma}[\boldsymbol{\xi}]\boldsymbol{n})\cdot\big(\boldsymbol{R}^T(\theta)\boldsymbol{e}_1\big) = 0 & \text{on} \quad \Gamma_C\times[0,T),\\
(\boldsymbol{\sigma}[\boldsymbol{\xi}]\boldsymbol{n})\cdot\big(\boldsymbol{R}^T(\theta)\boldsymbol{e}_2\big) \geq 0 & \text{on} \quad \Gamma_C\times[0,T),\\
\big((\mathbf{id}+\boldsymbol{\xi})\cdot\big(\boldsymbol{R}^T(\theta)\boldsymbol{e}_2\big)-g\big)\,(\boldsymbol{\sigma}[\boldsymbol{\xi}]\boldsymbol{n})\cdot\big(\boldsymbol{R}^T(\theta)\boldsymbol{e}_2\big) = 0 & \text{on} \quad \Gamma_C\times[0,T),\\
\boldsymbol{\xi}(\cdot,0) = \boldsymbol{\xi}^0 & \text{in} \quad \Omega,\\
\dot{\boldsymbol{\xi}}(\cdot,0) = \boldsymbol{\eta}^0 & \text{in} \quad \Omega,
\end{cases}
$$

where $\theta, g : [0,T) \to \mathbb{R}$ and $\boldsymbol{\xi}^0, \boldsymbol{\eta}^0$ are given functions, and $\boldsymbol{f}$ is defined by (2.8). (P) describes the complete set of equations of motion for $\boldsymbol{\xi}$ which we solve numerically in the remainder of this paper.

3 Numerical method

In this section, we describe and apply the discrete Morse flow (DMF) to discretize (P). The idea is to discretize (P) in time by using the implicit Crank-Nicolson scheme (Section 3.1). This yields a scheme where at each time step an elliptic obstacle problem needs to be solved. In Section 3.2 we derive a variational structure of this elliptic obstacle problem. In Section 3.3 we adjust the nonlinear conjugate gradient method to find a minimizer of the related minimization problem.

3.1 Time-discretized problem

For the discretization in time, let $T > 0$ be the end time, $M \in \mathbb{N}$ be the number of time steps, and $\Delta t := T/M$ be the time step size. For each time step $k = 0, 1, \cdots, M$, we set

$$\theta^k := \theta(k\Delta t), \quad g^k := g(k\Delta t),$$

and denote by $\boldsymbol{\xi}^k : \Omega \to \mathbb{R}^2$ the time-discretized approximation of the solution $\boldsymbol{\xi}$ of (P) at time $k\Delta t$. For convenience, we set $\boldsymbol{\xi}^k|_{k=-1} := \boldsymbol{\xi}^0 - \Delta t\boldsymbol{\eta}^0$.

Using the Crank-Nicolson scheme, we discretize the elastodynamics equation in time as

$$\rho\frac{\boldsymbol{\xi}^k - 2\boldsymbol{\xi}^{k-1} + \boldsymbol{\xi}^{k-2}}{(\Delta t)^2} = \mathbf{div}\,\boldsymbol{\sigma}\left[\frac{\boldsymbol{\xi}^k + \boldsymbol{\xi}^{k-2}}{2}\right] + \rho\boldsymbol{f}^{k-1} \quad \text{in } \Omega, \tag{3.1}$$

where we define

$$\boldsymbol{f}^{k-1}(\boldsymbol{x}) := \boldsymbol{f}\Big((k-1)\Delta t, \boldsymbol{x}, \boldsymbol{\xi}^{k-1}, (\boldsymbol{\xi}^{k-1} - \boldsymbol{\xi}^{k-2})/\Delta t\Big). \tag{3.2}$$

Using the definition of $\boldsymbol{f}$, (3.2) reads

$$\boldsymbol{f}^{k-1}(\boldsymbol{x}) = \ddot{\theta}^{k-1}\boldsymbol{R}(-\pi/2)(\boldsymbol{x} + \boldsymbol{\xi}^{k-1}) + (\dot{\theta}^{k-1})^2(\boldsymbol{x} + \boldsymbol{\xi}^{k-1}) + 2\dot{\theta}^{k-1}\boldsymbol{R}(-\pi/2)\frac{\boldsymbol{\xi}^{k-1} - \boldsymbol{\xi}^{k-2}}{\Delta t}.$$

In contrast to the purely implicit scheme used in previous works [10], the advantage of the Crank-Nicolson scheme is that it conserves the time-discrete energy in the case when $\theta \equiv 0$ with homogeneous Dirichlet boundary conditions. We introduce the notation $\boldsymbol{\sigma} : \boldsymbol{\varepsilon}$ to denote $\sigma_{ij}\varepsilon_{ij}$, namely

$$\boldsymbol{\sigma} : \boldsymbol{\varepsilon} := \sigma_{ij}\varepsilon_{ij}.$$

The following theorem is due to K.Švadlenka.

Theorem 1. *If $\theta \equiv 0$, $\boldsymbol{\xi}^k = \mathbf{0}$ on $\partial\Omega$ for $k = 0, 1, \cdots, M$, and $\boldsymbol{\xi}^k$ satisfies (3.1) for $k = 1, 2\cdots, M$, then the time-discrete energy*

$$E^k := \frac{1}{2}\int_\Omega \frac{|\boldsymbol{\xi}^k - \boldsymbol{\xi}^{k-1}|^2}{(\Delta t)^2}\,dx + \frac{1}{2}\int_\Omega \frac{\boldsymbol{\sigma}[\boldsymbol{\xi}^k] : \boldsymbol{\varepsilon}[\boldsymbol{\xi}^k] + \boldsymbol{\sigma}[\boldsymbol{\xi}^{k-1}] : \boldsymbol{\varepsilon}[\boldsymbol{\xi}^{k-1}]}{2}\,dx \quad \text{for } k = 1, 2, \cdots, M$$

does not depend on k.

Proof. Multiplying both sides of (3.1) by $\boldsymbol{\xi}^k - \boldsymbol{\xi}^{k-2}$, integrating over Ω and integrating by parts, we get

$$\int_\Omega \frac{\boldsymbol{\xi}^k - 2\boldsymbol{\xi}^{k-1} + \boldsymbol{\xi}^{k-2}}{(\Delta t)^2} \cdot (\boldsymbol{\xi}^k - \boldsymbol{\xi}^{k-2})\,dx = \int_\Omega \mathbf{div}\,\boldsymbol{\sigma}\left[\frac{\boldsymbol{\xi}^k + \boldsymbol{\xi}^{k-2}}{2}\right] \cdot (\boldsymbol{\xi}^k - \boldsymbol{\xi}^{k-2})\,dx,$$

$$\int_\Omega \frac{|\boldsymbol{\xi}^k|^2 - |\boldsymbol{\xi}^{k-2}|^2 - 2\boldsymbol{\xi}^k\cdot\boldsymbol{\xi}^{k-1} + 2\boldsymbol{\xi}^{k-1}\cdot\boldsymbol{\xi}^{k-2}}{(\Delta t)^2}\,dx = -\int_\Omega \frac{1}{2}\Big(\boldsymbol{\sigma}[\boldsymbol{\xi}^k] : \boldsymbol{\varepsilon}[\boldsymbol{\xi}^k] - \boldsymbol{\sigma}[\boldsymbol{\xi}^{k-2}] : \boldsymbol{\varepsilon}[\boldsymbol{\xi}^{k-2}]\Big)\,dx.$$

Summing over $k = 2$ to K, we obtain

$$E^1 = E^K$$

for $K = 2, 3, \cdots, M$. □

The Crank-Nicolson discretization above yields the following time-discretized scheme for (P). The choice of $(\boldsymbol{\xi}^k + \boldsymbol{\xi}^{k-2})/2$ in the boundary conditions is motivated by the variational formula that we explain in detail in the next subsection 3.2. Let $\boldsymbol{\xi}^0, \boldsymbol{\eta}^0 \in W^{1,2}(\Omega;\mathbb{R}^2)$ be given, and set $\boldsymbol{\xi}^k|_{k=-1} := \boldsymbol{\xi}^0 - \Delta t\boldsymbol{\eta}^0$. For $k = 1, 2, \cdots, M$, find $\boldsymbol{\xi}^k : \Omega \to \mathbb{R}^2$ such that the following equations

are satisfied:

$$(\mathrm{P}_k)\begin{cases} \rho\dfrac{\boldsymbol{\xi}^k-2\boldsymbol{\xi}^{k-1}+\boldsymbol{\xi}^{k-2}}{(\Delta t)^2}-\mathbf{div}\,\boldsymbol{\sigma}\left[\dfrac{\boldsymbol{\xi}^k+\boldsymbol{\xi}^{k-2}}{2}\right]=\rho\boldsymbol{f}^{k-1} & \text{in } \Omega,\\ \boldsymbol{\xi}^k=\mathbf{0} & \text{on } \Gamma_D,\\ (\mathbf{id}+\boldsymbol{\xi}^k)\cdot\left(\boldsymbol{R}^T(\theta^k)\boldsymbol{e}_2\right)\geq g^k & \text{on } \Gamma_C,\\ \left(\boldsymbol{\sigma}\left[\dfrac{\boldsymbol{\xi}^k+\boldsymbol{\xi}^{k-2}}{2}\right]\boldsymbol{n}\right)\cdot\left(\boldsymbol{R}^T(\theta^k)\boldsymbol{e}_1\right)=0 & \text{on } \Gamma_C,\\ \left(\boldsymbol{\sigma}\left[\dfrac{\boldsymbol{\xi}^k+\boldsymbol{\xi}^{k-2}}{2}\right]\boldsymbol{n}\right)\cdot\left(\boldsymbol{R}^T(\theta^k)\boldsymbol{e}_2\right)\geq 0 & \text{on } \Gamma_C,\\ \left((\mathbf{id}+\boldsymbol{\xi}^k)\cdot\left(\boldsymbol{R}^T(\theta^k)\boldsymbol{e}_2\right)-g^k\right)\left(\boldsymbol{\sigma}\left[\dfrac{\boldsymbol{\xi}^k+\boldsymbol{\xi}^{k-2}}{2}\right]\boldsymbol{n}\right)\cdot\left(\boldsymbol{R}^T(\theta^k)\boldsymbol{e}_2\right)=0 & \text{on } \Gamma_C,\\ \boldsymbol{\xi}^{-1}=\boldsymbol{\xi}^0-\Delta t\,\boldsymbol{\eta}^0 & \text{in } \Omega. \end{cases}$$

The convergence of the proposed numerical scheme based on the Crank-Nicolson time discretization is the subject of future work. However, the purely implicit time discretization was used previously to show the existence of a weak solution for a system of hyperbolic equations without a constraint in [9], and with constraint for a single equation in [10].

3.2 Variational structure of (P_k)

For any $k=1,2,\cdots,M$, problem (P_k) is an elliptic problem with an obstacle. It is the Euler-Lagrange equation for the minimizer of the functional

$$\mathscr{J}^k(\boldsymbol{\xi}):=\rho\int_\Omega\frac{|\boldsymbol{\xi}-2\boldsymbol{\xi}^{k-1}+\boldsymbol{\xi}^{k-2}|^2}{2(\Delta t)^2}\,dx+\frac{1}{2}\int_\Omega\left(\frac{1}{2}\boldsymbol{\sigma}[\boldsymbol{\xi}]+\boldsymbol{\sigma}[\boldsymbol{\xi}^{k-2}]\right):\boldsymbol{\varepsilon}[\boldsymbol{\xi}]\,dx-\rho\int_\Omega\boldsymbol{f}^{k-1}\cdot\boldsymbol{\xi}\,dx$$

over the admissible set

$$\mathscr{K}^k:=\left\{\boldsymbol{\xi}\in W^{1,2}(\Omega;\mathbb{R}^2);\ \boldsymbol{\xi}=\mathbf{0}\text{ a.e. on }\Gamma_D,\ (\mathbf{id}+\boldsymbol{\xi})\cdot\left(\boldsymbol{R}^T(\theta^k)\boldsymbol{e}_2\right)\geq g^k\text{ a.e. on }\Gamma_C\right\}.$$

Indeed, by calculating the first variation of $\mathscr{J}^k$ over $\mathscr{K}^k$ we obtain that any minimizer $\boldsymbol{\xi}^k$ satisfies (P_k). The existence of a unique minimizer follows from the facts that $\mathscr{J}^k$ is weakly lower-semicontinuous on $W^{1,2}(\Omega;\mathbb{R}^2)$, is bounded from below, has bounded sublevel sets, and that $\mathscr{K}^k$ is convex and closed in $W^{1,2}(\Omega;\mathbb{R}^2)$. Next we check, analogously to [7], that the sufficiently smooth minimizer $\boldsymbol{\xi}^k$ satisfies (P_k). The minimizer $\boldsymbol{\xi}^k$ satisfies the inequality

$$\mathscr{J}^k(\boldsymbol{\eta})\geq\mathscr{J}^k(\boldsymbol{\xi}^k)\qquad\text{for all }\boldsymbol{\eta}\in\mathscr{K}^k.$$

Taking any $\boldsymbol{\psi}\in C^\infty(\overline{\Omega};\mathbb{R}^2)$ such that $\boldsymbol{\eta}=\boldsymbol{\xi}^k+s\boldsymbol{\psi}\in\mathscr{K}^k$ for small $s\geq 0$ and expanding $\mathscr{J}^k(\boldsymbol{\xi}^k+s\boldsymbol{\psi})$ in terms of s, we deduce that the first-order term in s must be non-negative, that is,

$$\rho\int_\Omega\frac{(\boldsymbol{\xi}^k-2\boldsymbol{\xi}^{k-1}+\boldsymbol{\xi}^{k-2})\cdot\boldsymbol{\psi}}{(\Delta t)^2}\,dx+\int_\Omega\boldsymbol{\sigma}\left[\frac{\boldsymbol{\xi}^k+\boldsymbol{\xi}^{k-2}}{2}\right]:\boldsymbol{\varepsilon}[\boldsymbol{\psi}]\,dx-\rho\int_\Omega\boldsymbol{f}^{k-1}\cdot\boldsymbol{\psi}\,dx\geq 0.$$

Integrating by parts, we have

$$\begin{aligned} 0 \leq \quad & \int_\Omega \left(\rho \frac{(\boldsymbol{\xi}^k - 2\boldsymbol{\xi}^{k-1} + \boldsymbol{\xi}^{k-2})}{(\Delta t)^2} - \mathbf{div}\, \boldsymbol{\sigma} \left[\frac{\boldsymbol{\xi}^k + \boldsymbol{\xi}^{k-2}}{2} \right] - \rho \boldsymbol{f}^{k-1} \right) \cdot \boldsymbol{\psi}\, dx \\ & + \int_{\Gamma_C} \left(\boldsymbol{\sigma} \left[\frac{\boldsymbol{\xi}^k + \boldsymbol{\xi}^{k-2}}{2} \right] \boldsymbol{n} \right) \cdot \boldsymbol{\psi}\, ds. \end{aligned} \tag{3.3}$$

Choosing $\boldsymbol{\psi} \in C_0^\infty(\Omega; \mathbb{R}^2)$, (3.3) implies the first equation in (P_k). Thus for $\boldsymbol{\psi} \in C^\infty(\overline{\Omega}; \mathbb{R}^2)$, we deduce from (3.3)

$$\begin{aligned} 0 & \leq \int_{\Gamma_C} \left(\boldsymbol{\sigma} \left[\frac{\boldsymbol{\xi}^k + \boldsymbol{\xi}^{k-2}}{2} \right] \boldsymbol{n} \right) \cdot \boldsymbol{\psi}\, ds \\ & = \int_{\Gamma_C} \sum_{i=1}^{2} \left\{ \left(\boldsymbol{\sigma} \left[\frac{\boldsymbol{\xi}^k + \boldsymbol{\xi}^{k-2}}{2} \right] \boldsymbol{n} \right) \cdot \left(\boldsymbol{R}^T(\theta^k) \boldsymbol{e}_i \right) \right\} \left\{ \boldsymbol{\psi} \cdot \left(\boldsymbol{R}^T(\theta^k) \boldsymbol{e}_i \right) \right\} ds. \end{aligned} \tag{3.4}$$

By choosing $\boldsymbol{\psi}$ such that

$$\boldsymbol{\psi} \cdot \left(\boldsymbol{R}^T(\theta^k) \boldsymbol{e}_2 \right) = 0 \quad \text{on } \Gamma_C,$$

we obtain the fourth equation of (P_k). By choosing $\boldsymbol{\psi}$ such that

$$\boldsymbol{\psi} \cdot \left(\boldsymbol{R}^T(\theta^k) \boldsymbol{e}_2 \right) \geq 0 \quad \text{on } \Gamma_C,$$

we obtain $\boldsymbol{\eta} = \boldsymbol{\xi}^k + s\boldsymbol{\psi} \in \mathscr{K}^k$ for small $s \geq 0$, which by (3.4) yields the fifth equation of (P_k). Finally, suppose that $(\mathbf{id} + \boldsymbol{\xi}^k) \cdot \left(\boldsymbol{R}^T(\theta^k) \boldsymbol{e}_2 \right) - g^k > 0$ at a point $\boldsymbol{x} \in \Gamma_C$. Then there exists $\boldsymbol{\psi} \in C^\infty(\overline{\Omega}; \mathbb{R}^2)$ such that

$$\boldsymbol{\psi} \cdot \left(\boldsymbol{R}^T(\theta^k) \boldsymbol{e}_2 \right)(\boldsymbol{x}) < 0 \quad \text{and} \quad (\mathbf{id} + \boldsymbol{\xi}^k + s\boldsymbol{\psi}) \cdot \left(\boldsymbol{R}^T(\theta^k) \boldsymbol{e}_2 \right) - g^k \geq 0 \quad \text{on } \Gamma_C \text{ for small } s \geq 0.$$

Condition (3.4) together with the fifth equation implies

$$\left(\boldsymbol{\sigma} \left[\frac{\boldsymbol{\xi}^k(\boldsymbol{x}) + \boldsymbol{\xi}^{k-2}(\boldsymbol{x})}{2} \right] \boldsymbol{n}(\boldsymbol{x}) \right) \cdot \left(\boldsymbol{R}^T(\theta^k) \boldsymbol{e}_2 \right) = 0,$$

and therefore the last equation in (P_k) holds.

3.3 Numerical method for solving the minimization problem

The aim is to minimize $\mathscr{J}^k$ over $\mathscr{K}^k$ numerically using the finite element method.

Given a space discretization parameter $\Delta x > 0$, we approximate the domain Ω by a triangular mesh with corresponding domain $\widetilde{\Omega}$. To do this, we first distribute equispaced nodes of distance approximately Δx on Γ_D and Γ_C, and then we generate the interior nodes by applying the Poisson disk sampling algorithm by [13] with parameter $r = \frac{2}{3}\Delta x$. The triangular mesh is then given by the Delaunay triangulation [12] on the constructed nodes.

We approximate the minimizer of $\mathscr{J}^k$ by a continuous function on $\widetilde{\Omega}$ which is linear on each element of the mesh. We denote the space of such functions by V. Let $N \in \mathbb{N}$ be the number of the nodes, $\{\boldsymbol{x}_n\}_{n=1}^N$ be the nodes, and I_D and I_C be defined by

$$I_D := \{n\,;\, \boldsymbol{x}_n \in \Gamma_D\}, \quad I_C := \{n\,;\, \boldsymbol{x}_n \in \Gamma_C\}.$$

We define the basis functions $\zeta_n : \mathbb{R}^2 \to \mathbb{R}$ as the continuous functions, which are linear on each element and satisfy

$$\zeta_n(\boldsymbol{x}_m) = \delta_{nm}. \tag{3.5}$$

For the vector

$$\widetilde{\boldsymbol{\xi}} = (\widetilde{\xi}_{1,1}, \widetilde{\xi}_{1,2}, \cdots, \widetilde{\xi}_{1,N}, \widetilde{\xi}_{2,1}, \cdots, \widetilde{\xi}_{2,N}) \in \mathbb{R}^{2N},$$

we define the operator $P : \mathbb{R}^{2N} \to V$ as

$$P(\widetilde{\boldsymbol{\xi}})(\boldsymbol{x}) := \left(\sum_{n=1}^{N} \widetilde{\xi}_{1,n} \zeta_n(\boldsymbol{x}), \sum_{n=1}^{N} \widetilde{\xi}_{2,n} \zeta_n(\boldsymbol{x}) \right).$$

We set $\widetilde{\boldsymbol{\xi}}^0, \widetilde{\boldsymbol{\xi}}^{-1} \in \mathbb{R}^{2N}$ as

$$\widetilde{\xi}^0_{d,n} := \xi^0_d(\boldsymbol{x}_n), \quad \widetilde{\xi}^{-1}_{d,n} := \xi^{-1}_d(\boldsymbol{x}_n)$$

for $d = 1,2$, $n = 1,2,\cdots,N$. Then for any $k = 1,2,\cdots,M$, we seek inductively a minimizer $\widetilde{\boldsymbol{\xi}}^k$ of the discrete functional

$$\begin{aligned}\widetilde{\mathscr{J}}^k(\widetilde{\boldsymbol{\xi}}) := \rho \int_{\widetilde{\Omega}} \frac{\left| P(\widetilde{\boldsymbol{\xi}}) - 2P(\widetilde{\boldsymbol{\xi}}^{k-1}) + P(\widetilde{\boldsymbol{\xi}}^{k-2}) \right|^2}{2(\Delta t)^2} dx + \frac{1}{2} \int_{\widetilde{\Omega}} \left(\frac{1}{2} \boldsymbol{\sigma}[P(\widetilde{\boldsymbol{\xi}})] + \boldsymbol{\sigma}[P(\widetilde{\boldsymbol{\xi}}^{k-2})] \right) : \boldsymbol{\varepsilon}[P(\widetilde{\boldsymbol{\xi}})]\, dx \\ - \rho \int_{\widetilde{\Omega}} \boldsymbol{f} \left((k-1)\Delta t, \cdot, P(\widetilde{\boldsymbol{\xi}}^{k-1}), (P(\widetilde{\boldsymbol{\xi}}^{k-1}) - P(\widetilde{\boldsymbol{\xi}}^{k-2}))/\Delta t \right) \cdot P(\widetilde{\boldsymbol{\xi}})\, dx\end{aligned}$$

over the admissible set

$$\widetilde{\mathscr{K}}^k := \left\{ \widetilde{\boldsymbol{\xi}} \in \mathbb{R}^{2N};\, \widetilde{\xi}_{1,n} = \widetilde{\xi}_{2,n} = 0 \text{ for } n \in I_D, (\boldsymbol{x}_n + (\widetilde{\xi}_{1,n}, \widetilde{\xi}_{2,n})) \cdot \left(\boldsymbol{R}^T(\theta^k) \boldsymbol{e}_2 \right) \geq g^k \text{ for } n \in I_C \right\}.$$

For fixed $k \geq 1$, we approximate the minimizer of the functional $\widetilde{\mathscr{J}}^k$ in the admissible set $\widetilde{\mathscr{K}}^k$ using a variant of the nonlinear conjugate gradient method with a projection given by the following steps ($\varepsilon > 0$ is a given stopping tolerance):

(1) initial guess $\widetilde{\boldsymbol{\xi}}_0 \in \widetilde{\mathscr{K}}^k$ (for example, $\widetilde{\boldsymbol{\xi}}_0 = \mathrm{Proj}_{\widetilde{\mathscr{K}}^k}(\widetilde{\boldsymbol{\xi}}^{k-1})$)

(2) $\boldsymbol{g}_1 = -\nabla \widetilde{\mathscr{J}}^k(\widetilde{\boldsymbol{\xi}}_0)$

(3) $\boldsymbol{p}_1 = T^k_{\widetilde{\boldsymbol{\xi}}_0}(\boldsymbol{g}_1)$

(4) $e = \|\boldsymbol{p}_1\|$; if $e \leq \varepsilon$, then set $\widetilde{\boldsymbol{\xi}}^k = \widetilde{\boldsymbol{\xi}}_0$ and proceed to the next time step $k+1$

(5) For $m = 1,2,\ldots$:

(i) $\alpha_m = \mathrm{argmin}_{\alpha>0} \widetilde{\mathscr{J}}^k(\widetilde{\boldsymbol{\xi}}_{m-1} + \alpha \boldsymbol{p}_m)$ (Exact solution as the function is quadratic)

(ii) $\widetilde{\boldsymbol{\xi}}_m = \mathrm{Proj}_{\widetilde{\mathscr{K}}^k}(\widetilde{\boldsymbol{\xi}}_{m-1} + \alpha_m \boldsymbol{p}_m)$

(iii) $\boldsymbol{g}_{m+1} = -\nabla \widetilde{\mathscr{J}}^k(\widetilde{\boldsymbol{\xi}}_m)$

(iv) $\beta_m = \max\left\{ 0, \frac{(\boldsymbol{g}_{m+1} - \boldsymbol{g}_m) \cdot \boldsymbol{g}_{m+1}}{\|\boldsymbol{g}_m\|^2} \right\}$

(v) $\boldsymbol{p}_{m+1} = T^k_{\widetilde{\boldsymbol{\xi}}_m}(\boldsymbol{g}_{m+1} + \beta_m \boldsymbol{p}_m)$

(vi) $e = \|T^k_{\widetilde{\boldsymbol{\xi}}_m}(\boldsymbol{g}_{m+1})\|$; if $e \leq \varepsilon$, then set $\widetilde{\boldsymbol{\xi}}^k = \widetilde{\boldsymbol{\xi}}_m$ and proceed to the next time step $k+1$,

where

$$\left(\mathrm{Proj}_{\widetilde{\mathscr{K}}^k}(\widetilde{\boldsymbol{\xi}})\right)_{(n,n+N)} := \begin{cases} (\widetilde{\xi}_{1,n},\widetilde{\xi}_{2,n}) - \min\left\{0, g^k - (\boldsymbol{x}_n + (\widetilde{\xi}_{1,n},\widetilde{\xi}_{2,n}))\cdot(\boldsymbol{R}^T(\theta^k)\boldsymbol{e}_2)\right\}(\boldsymbol{R}^T(\theta^k)\boldsymbol{e}_2) & \text{if } n \in I_C, \\ (\widetilde{\xi}_{1,n},\widetilde{\xi}_{2,n}) & \text{otherwise} \end{cases}$$

for any $\widetilde{\boldsymbol{\xi}} \in \mathbb{R}^{2N}$ and

$$\left(T^k_{\widetilde{\boldsymbol{\xi}}}(\boldsymbol{p})\right)_{(n,n+N)} := \begin{cases} (p_{1,n},p_{2,n}) - \min\left\{0, (p_{1,n},p_{2,n})\cdot(\boldsymbol{R}^T(\theta^k)\boldsymbol{e}_2)\right\}(\boldsymbol{R}^T(\theta^k)\boldsymbol{e}_2) & \\ \qquad \text{if } n \in I_C \text{ and } (\boldsymbol{x}_n + (\widetilde{\xi}_{1,n},\widetilde{\xi}_{2,n}))\cdot(\boldsymbol{R}^T(\theta^k)\boldsymbol{e}_2) \le g^k, & \\ (p_{1,n},p_{2,n}) \qquad \text{otherwise} & \end{cases}$$

for any $\boldsymbol{p} \in \mathbb{R}^{2N}$. The operator $\mathrm{Proj}_{\widetilde{\mathscr{K}}^k}$ is the orthogonal projection onto the set $\widetilde{\mathscr{K}}^k$. The operator $T^k_{\widetilde{\boldsymbol{\xi}}}(\boldsymbol{p})$ restricts the search direction $(\boldsymbol{p})_{(n,n+N)}$ for $n \in I_C$ so that no jump over the obstacle g^k occurs.

4 Numerical results

In this section we present numerical results based on the method proposed in Section 3. We choose the domain Ω as the annulus

$$\Omega := \{\boldsymbol{x} \in \mathbb{R}^2;\, r_D < |\boldsymbol{x}| < r_C\}, \quad \Gamma_D := \{\boldsymbol{x} \in \mathbb{R}^2;\, |\boldsymbol{x}| = r_D\}, \quad \Gamma_C := \{\boldsymbol{x} \in \mathbb{R}^2;\, |\boldsymbol{x}| = r_C\},$$

where $r_D = 0.25$ and $r_C = 0.5$. We further set the initial data as $\boldsymbol{\xi}^0 = \boldsymbol{0}$ and $\boldsymbol{\eta}^0 = \boldsymbol{0}$. The Lamé constants are given by

$$\lambda = \frac{E\nu}{(1+\nu)(1-2\nu)}, \quad \mu = \frac{E}{2(1+\nu)},$$

where E and ν are Young's modulus and Poisson's ratio, respectively. We denote by Δx the mesh size. Table 1 shows the reference values of the involved parameters.

Table 1: Reference values for the parameters involved in the simulations.

E	ν	ρ	ω	Δx
0.1	0.49	1	$\pi/10$	0.0125

We simulate two cases. In the first case we remove the obstacle, and study the sensitivity of the roller's dynamics with respect to the parameters. In particular, we are interested in the vibrations in the radial and tangential displacements, because understanding such vibrations is important for removing the squeaking sound of printer rollers. As feedback on these simulations, we add a vibration to the given rotation $\theta(t)$ to investigate the occurrence of resonance.

In the second case we add the obstacle. We are interested in the shape of the deformed domain and the size of the stress tensor $\boldsymbol{\sigma}[\boldsymbol{\xi}]$ as a function on the deformed domain, especially in the region close to the contact zone.

The case without an obstacle We set g small enough to remove any effect from the obstacle. We are interested in the average radial displacement R and the average tangential displacement α of the roller defined by

$$R(t) = \frac{1}{|\Gamma_C|}\int_{\Gamma_C} \frac{\boldsymbol{\xi}(\boldsymbol{x},t)\cdot\boldsymbol{x}}{|\boldsymbol{x}|}\,ds, \tag{4.1}$$

$$\alpha(t) = \frac{1}{|\Gamma_C|}\int_{\Gamma_C} \frac{\boldsymbol{\xi}(\boldsymbol{x},t)\cdot\boldsymbol{x}^{\perp}}{|\boldsymbol{x}|}\,ds. \tag{4.2}$$

We set the parameter values as in Table 1 unless mentioned otherwise.

In the first set of simulations, we consider the four values $\Delta x = \Delta x_i := 2^{i-1}\Delta\widetilde{x}$ for $i = 1,2,3,4$, $\Delta\widetilde{x} := 0.0125$ and set the corresponding time step size as $\Delta t = \Delta x$. We consider a linear time-dependence for the rotation angle given by

$$\theta(t) = \omega t.$$

Figures 3 and 4 show the corresponding graphs of $R(t)$ and $\alpha(t)$, which resemble waves. These waves correspond to the vibration modes in the radial and tangential directions (see [14]). We estimate the periods of the first modes by assuming that the roller can be approximated by a infinite strip of thickness $d = r_C - r_D$ of an elastic material whose one side is fixed (boundary Γ_D) and the other is free to move (boundary Γ_C). From this assumption, we observe that the first mode has wavelength $\Lambda \approx 4d$. The wavelength is related to the period τ as $\Lambda = c\tau$, where c is the speed of sound. Our elastic material has primary (pressure) and secondary (shear) waves with speeds

$$c_p = \sqrt{\frac{\lambda+2\mu}{\rho}}, \qquad c_s = \sqrt{\frac{\mu}{\rho}}, \tag{4.3}$$

which yield for our parameters

$$\tau_p = \frac{4d}{c_p} \approx 0.764, \qquad \tau_s = \frac{4d}{c_s} \approx 5.46.$$

The short period wave therefore corresponds to the radial vibration mode (primary wave) and the long period wave corresponds to the tangential vibration mode (secondary wave). The radial vibration is initiated by the centrifugal force. Once there is a motion in the radial direction, the Coriolis effect causes the tangential vibration.

Firstly, we observe that the amplitude of the waves does not change in time. We expect this from Theorem 1, which shows in a simplified setting that the time-discrete energy is conserved. Secondly, we observe a phase-shift when Δx varies. The phase-shift decreases as Δx decreases. It is curious that the phase shift of $\alpha(t)$ is much higher than the phase shift of $R(t)$; we did not find an explanation for this effect.

In the next set of simulations, we vary Young's modulus by $E = E_i := 2^{i-1}\widetilde{E}$ ($i = 1,2,3, \widetilde{E} := 0.05$). Figures 5 and 6 show the graphs of $R(t)$ and $\alpha(t)$ again. Firstly, we observe that the amplitude of the wave of $R(t)$ is halved when E is doubled, which is expected from the physical meaning of Young's modulus. Secondly, the frequency of the wave of $R(t)$ seems to scale as the square root of E, which we expect from (4.3). Thirdly, we observe that the amplitude of the wave of $\alpha(t)$ decreases when E increases. Indeed, since the amplitude of the radial wave decreases with increasing E and the tangential vibration is caused by the Coriolis effect whose magnitude depends on the radial velocity, as discussed above, this is the expected behavior. Finally, the frequency of the wave of $\alpha(t)$ seems to scale as the square root of E, which we expect from (4.3).

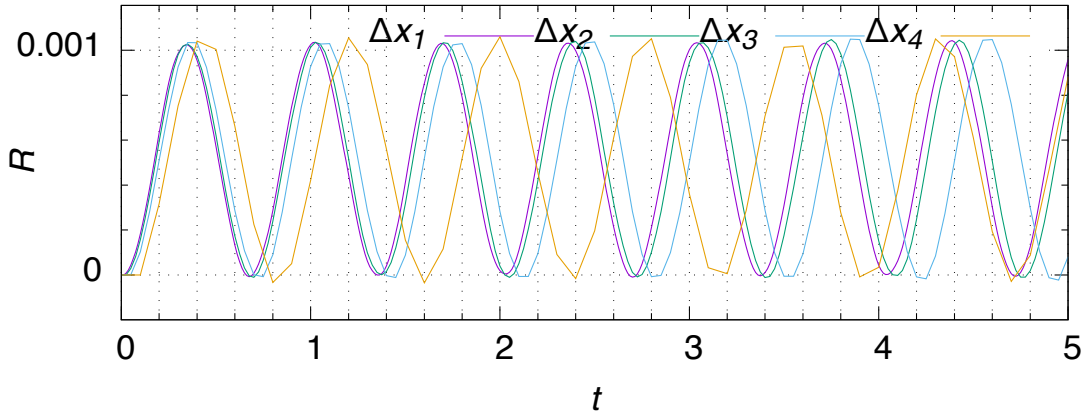

Figure 3: The average radial displacement $R(t)$ (see (4.1)) as a function of time for four values of the mesh size Δx.

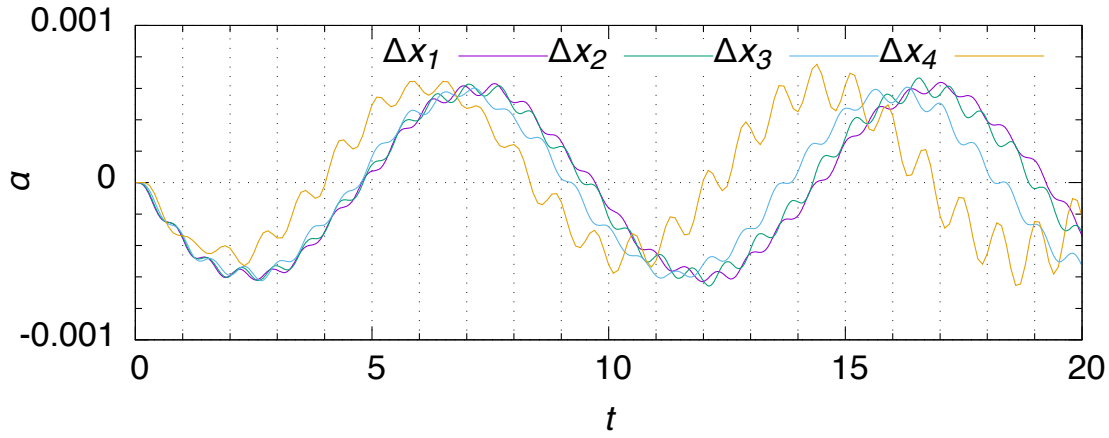

Figure 4: The average tangential displacement $\alpha(t)$ (see (4.2)) as a function of time for four values of the mesh size Δx.

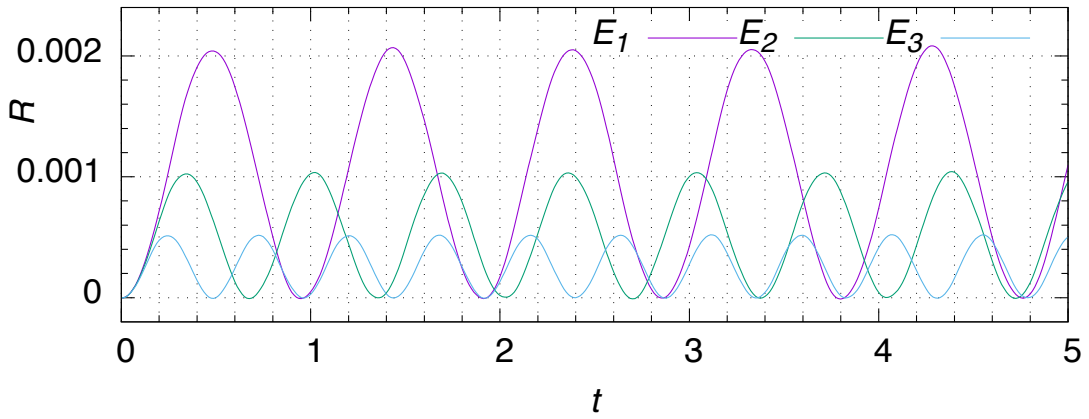

Figure 5: The graph of $R(t)$ for three values of Young's modulus E.

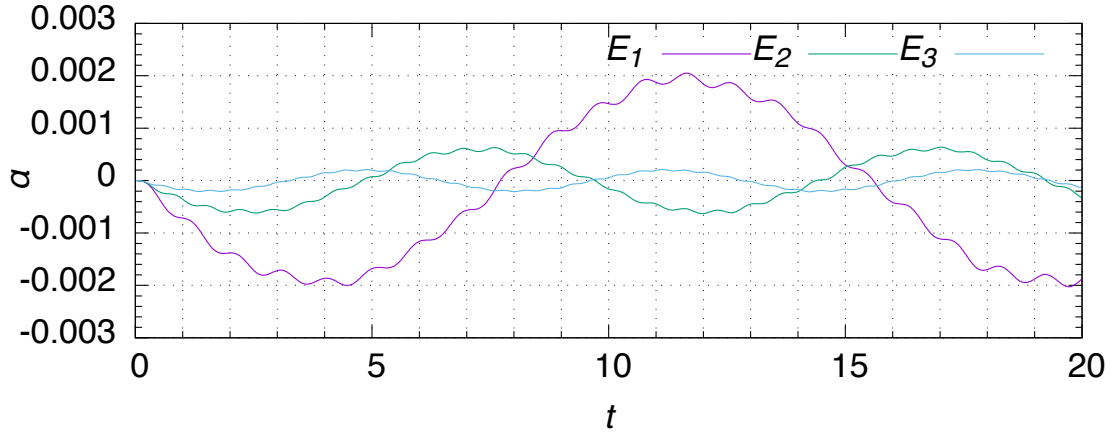

Figure 6: The graph of $\alpha(t)$ for three values of Young's modulus E.

In the final simulation for the roller without obstacle, we try to enforce resonance by perturbing the rotation angle by a wave, i.e., we set

$$\theta(t) = \omega t + a\cos(bt). \tag{4.4}$$

Based on Figure 6, the period of α is approximately 9.75 when $E = E_2$. We set $b = 2\pi/9.75$ for the frequency of the perturbation. We choose $a = 0.001$ for the amplitude to ensure that the perturbation only amounts to a small contribution to $\dot{\theta}(t)$. Figure 7 shows the resulting graph of $\alpha(t)$. Even though the perturbation is small, we observe a significant increase in the amplitude of $\alpha(t)$ over time. Such resonance effect can be the key for understanding the squeaking sound of rollers.

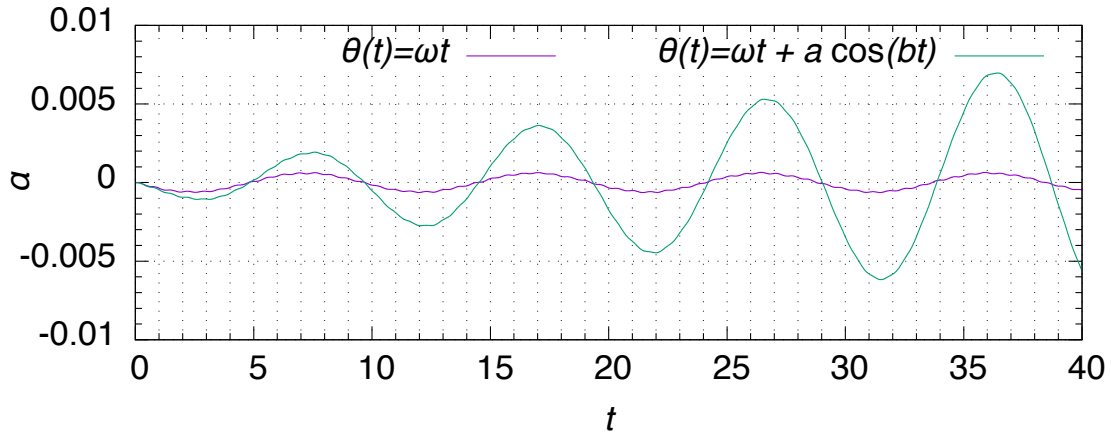

Figure 7: The graph of $\alpha(t)$ for the perturbed rotation given by (4.4). The graph in Figure 4 is repeated here for reference.

The case with an obstacle We set the height of the obstacle g as

$$g(t) = \min\left\{0.005t, \frac{r_C - r_D}{10}\right\} - r_C.$$

For this choice, at $t = 0$, the contact zone between the obstacle and the deformed configuration is a single point. Then, the obstacle compresses the roller by moving upwards with constant velocity until the time t at which $g(t) = \frac{r_C - r_D}{10} - r_C$ remains constant.

It turns out that the obstacle creates high frequency waves in the stress field in Ω. To suppress these waves, we add a damping term to the energy functional $\mathscr{J}^k$:

$$\mathscr{J}^k_\eta(\boldsymbol{\xi}) := \mathscr{J}^k(\boldsymbol{\xi}) + \eta \int_\Omega \frac{|\boldsymbol{\xi} - \boldsymbol{\xi}^{k-2}|^2}{4\Delta t}\, dx,$$

where we set $\eta = 1$. The corresponding change to $(\mathrm{P_k})$ is that the first equation is replaced by

$$\rho \ddot{\boldsymbol{\xi}} + \eta \dot{\boldsymbol{\xi}} = \mathbf{div}\boldsymbol{\sigma}[\boldsymbol{\xi}] + \rho \boldsymbol{f}(\cdot, \cdot, \boldsymbol{\xi}, \dot{\boldsymbol{\xi}}) \quad \text{in } \Omega \times (0, T).$$

Figures 8 and 9 illustrate the magnitude of the stress defined by

$$|\boldsymbol{\sigma}| := \sqrt{\sigma_{ij}^2} \tag{4.5}$$

on the deformed configuration. In the simulations, we consider the two values $\omega = 0, \pi/10$. Figure 8 illustrates the simple compression ($\omega = 0$). The shock of the contact of the obstacle propagates symmetrically. When the obstacle is more tightly pressed to the roller, the stress is concentrated near the contact zone.

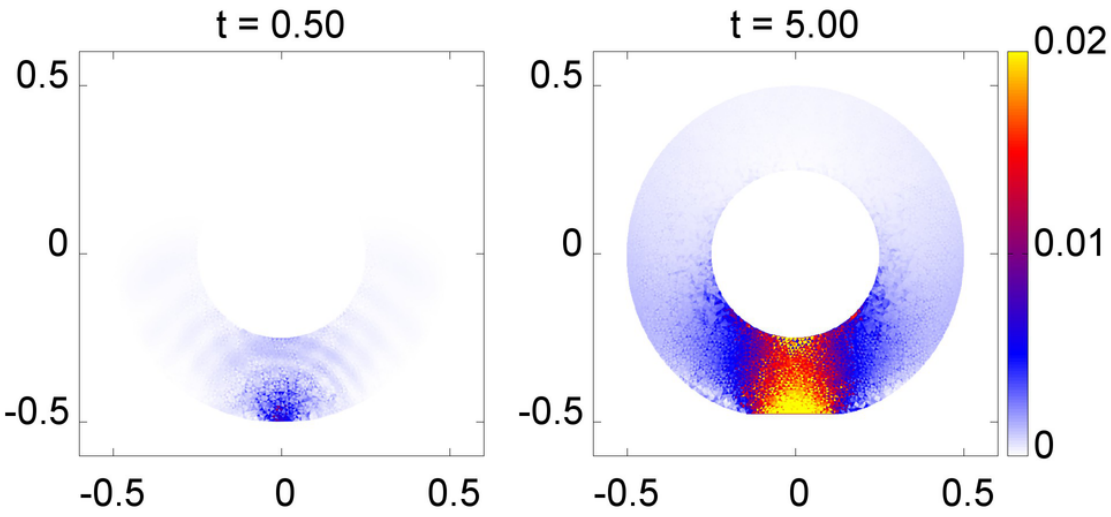

Figure 8: Simple compression ($\omega = 0$). Here, the magnitude of the stress (see (4.5)) is displayed.

In Figure 9, we observe that the stress is initially concentrated near the boundary Γ_D; this is natural for Dirichlet boundary conditions. The shock propagates more rapidly in the direction of the rotation. We conjecture that the complicated stress distribution at $t = 5$ is caused by the interaction of the radial waves (see Figures 3 and 5) with the forced compression by the obstacle.

Conclusion Based on these numerical results, the proposed method shows promise to help with the understanding of the source of the squeaking sound in a scanner's roller. An implementation that includes the stick-slip friction force at the contact zone is under development.

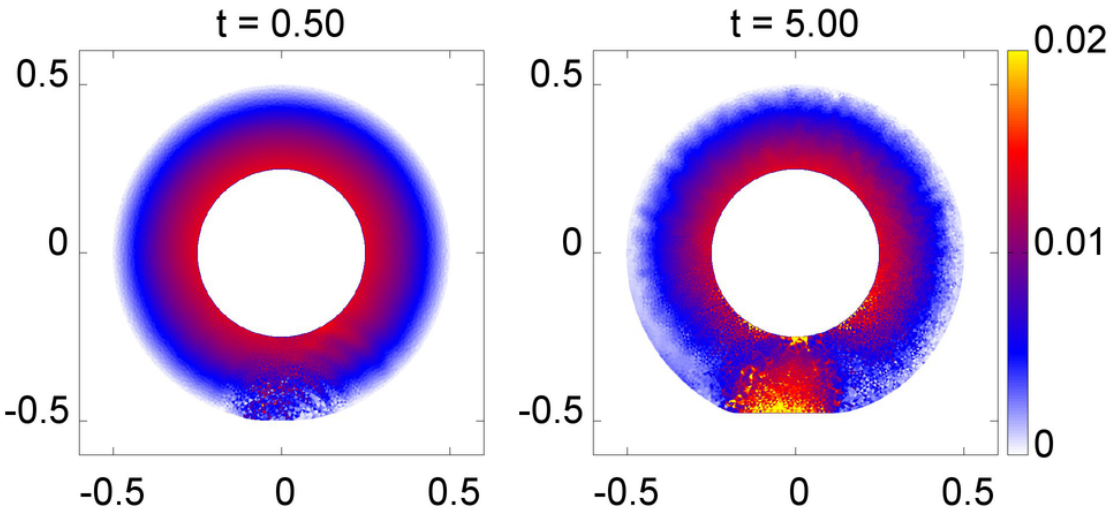

Figure 9: The direction of rotation is counter-clockwise with the rotation speed $\omega = \pi/10$. The magnitude of the stress (see (4.5)) is displayed.

References

[1] A. Signorini, *Sopra alcune questioni di statica dei sistemi continui*, Annali della Scuola Normale Superiore di Pisa **2**, (1933), 231–251.

[2] J.L. Lions, G. Stampacchia, *Variational inequalities*, Commun. Pure Appl. Math. **20**, (1967), 493–519.

[3] J.T. Oden, T.L. Lin, *On the general rolling contact problem for finite deformations of a viscoelastic cylinder*, Comput. Methods Appl. Mech. Engrg. **57** (1986), 297–367.

[4] N. Kikuchi, J.T. Oden, *Contact Problems in Elasticity: A Study of Variational Inequalities and Finite Element Methods*, SIAM, Philadelphia (1988).

[5] G.Ḧu, P. Wriggers, *On the adaptive finite element method of steady-state rolling contact for hyperelasticity in finite deformations*, Comput. Methods Appl. Mech. Engrg. **191** (2002), 1333–1348.

[6] T.A. Laursen, *Computational Contact and Impact Mechanics*, Springer-Verlag, New York (2002).

[7] I. Hlaváček, J. Haslinger, J. Nečas, J. Lovíšek, *Solution of Variational Inequalities in Mechanics*, Springer, New York (1988)

[8] N. Kikuchi, *An approach to the construction of Morse flows for variational functionals*, Nematics - Mathematical and Physical Aspects, Nato Adv. Sci. Inst. Ser. C: Math. Phys. Sci. **332**, Kluwer Acad. Publ., Dodrecht-Boston-London (1991), 195–198.

[9] A. Tachikawa, *A variational approach to constructing weak solutions of semilinear hyperbolic systems*, Adv. Math. Sci. Appl. **4**, (1994), 93–103.

[10] K. Švadlenka, S. Omata, *Mathematical modelling of surface vibration with volume constraint and its analysis*, Nonlinear Analysis, **69** (9), 2008, 3202–3212.

[11] D. Dunbar, G. Humphreys, *A spatial data structure for fast Poisson-disk sample generation*, ACM Trans. Graph. **25** (3), 2006, 503–508.

[12] J.R. Shewchuk, *Delaunay Mesh Generation*, Chapter 2, Lecture Notes at Department of Electrical Engineering and Computer Sciences, University of California at Berkeley, CA 94720 on February 5, 2012.

[13] R. Bridson, *Fast Poisson Disk Sampling in Arbitrary Dimensions*, ACM SIGGRAPH 2007 sketches Article No. 22, 2007.

[14] G. Ambati, J.F. W.Bell, J.C.K. Sharp, *In-Plane Vibrations of Annular Rings*, Journal of Sound and Vibration **47**(3), 1976, 415–432.